Surface & Coatings Technology 360 (2019) 329–334

Contents lists available at ScienceDirect

Surface & Coatings Technology

journal homepage: www.elsevier.com/locate/surfcoat

The formation of a homogeneous α-alumina coating on a Ni-based superalloy from a layer stack deposited by cathodic arc evaporation

J. Ast[a,*], Z. Balogh-Michels[b], M. Döbeli[c], A. Dommann[b], M. Gindrat[d], X. Maeder[a], A. Neels[b], M.N. Polyakov[a], H. Rudigier[e], B. Widrig[e], J. Ramm[e]

[a] Laboratory for Mechanics of Materials and Nanostructures, Empa, Feuerwerkerstrasse 39, 3602 Thun, Switzerland
[b] Center for X-ray Analytics, Empa, Überlandstrasse 129, CH-8600 Dübendorf, Switzerland
[c] Ion Beam Physics, ETH Zurich, Otto-Stern-Weg 5, CH-8093 Zürich, Switzerland
[d] Oerlikon Metco AG, 5610 Wohlen, Switzerland
[e] Oerlikon Surface Solutions AG, Iramali 18, LI-9496 Balzers, Liechtenstein

ARTICLE INFO

Keywords:
Cathodic arc evaporation
thermal barrier coating
Transmission Kikuchi Diffraction
Rutherford Backscattering Spectrometry
Ni-based superalloy
X-ray diffraction

ABSTRACT

Cathodic arc evaporation was applied to form a layer stack on a Ni-based superalloy single crystalline substrate in a single in-situ vacuum deposition process. The initial layer was deposited using a target with the same nominal composition as the superalloy substrate. Subsequently, a second layer was deposited using a target with a composition of 70 at.% Al and 30 at.% Cr, and the deposition was conducted in flowing oxygen to form Al-Cr-O. The thermal stability of the layer stack was investigated by means of a heat treatment at 1100 °C in air. The substrate-like coating recrystallized at elevated temperature and showed epitaxial growth on the superalloy single crystal, according to transmission Kikuchi diffraction measurements. A thin layer of pure α-alumina formed on top of the substrate-like coating and a compact Al-Cr-O phase with corundum structure developed towards the top of the coating. Microstructural and chemical analyses of the coating architectures in the as-deposited and annealed states were performed by means of transmission electron microscopy, energy dispersive X-ray spectroscopy, X-ray diffraction and Rutherford backscattering spectrometry, and utilized to explain the recrystallization and diffusion processes in the layer stack.

1. Introduction

The past decades showed an impressive development of high-temperature stable superalloys [1,2]. This progress was mainly triggered by the demand for increased operating temperatures of land-based and aero turbines to increase their efficiency. Among these materials, Ni-based superalloys are dominant and manufacturing and the properties of these materials have been investigated [3–5]. The development resulted in materials with increased creep resistance at higher temperatures [6–9]. Higher operating temperatures, however, require improved surface stability of the components with respect to oxidation and corrosion. This is difficult to achieve with existing Ni-based superalloy bulk material. Consequently, the surface needs protection by thermal barrier coatings [10,11]. In the current state-of-the-art, the coatings applied to the superalloy surface form a well-adhered and stable interface towards the substrate by diffusion processes at elevated temperatures and create a protective oxide at their surface or at the interface with the next layer in the coating stack. The function of the coating is to provide the diffusing elements, which are necessary to form adherent interfaces and protective oxides. The selection of a specific coating depends on many parameters. Of particular importance is the adaptation to the bulk material which should be protected and the conditions under which the component will be operated, especially temperature and environment. Two types of coatings are particularly important: diffusion aluminide coatings [12] and overlay coatings [13]. The former are produced by pack cementation or chemical vapour deposition (CVD) techniques. Aluminum is applied to the bulk surface and diffuses to the bulk, forming the β-NiAl phase. MCrAlY (M = Ni, Co, or NiCo) overlay coatings are typically applied by spray technology and form β-NiAl and γ′-Ni_3Al or γ-phases. For both coating types, the adhesion to the bulk substrate is ensured by a high temperature annealing step and the α-Al_2O_3 scaling at the surface of the coating is utilized as an oxidation or corrosion barrier.

If the operating temperature at the surface of the bulk material is higher than the stability of the superalloy, the protective coating stack has to provide – in addition to oxidation and corrosion barrier function -

* Corresponding author.
E-mail address: johannes.ast@empa.ch (J. Ast).

https://doi.org/10.1016/j.surfcoat.2018.12.089
Received 17 October 2018; Received in revised form 20 December 2018; Accepted 21 December 2018
Available online 22 December 2018

the temperature drop, which is necessary for the stability of the bulk material. For such applications, the MCrAlY overlay coating is typically coated with an additional Yttrium-stabilized Zirconia (YSZ) layer that is several hundred microns in thickness. This coating stack is referred to as the Thermal Barrier Coating (TBC) [14,15]. In this coating combination, the interface between the MCrAlY bond coat (BC) and the porous YSZ is of particular importance, because it must guarantee the mechanical stability between the metallic BC and the YSZ and, in addition, it must provide an excellent diffusion barrier to protect the MCrAlY from oxidation. This is achieved by a thermally grown oxide (TGO) at the surface of the MCrAlY before the deposition with YSZ and a further stabilization of this TGO by oxygen transport through the YSZ.

In this work, an approach for an oxidation barrier is investigated, which is based upon an overlay coating deposited by cathodic arc evaporation (CAE), a physical vapour deposition (PVD) technique. In contrast to standard MCrAlY overlay coatings, the PVD layer stack presented here is much thinner. It consists of a first layer - the substrate-like coating – which is intended to have nearly the same chemical composition as the bulk substrate. It would be beneficial for good coating adhesion and the suppression of void formation if this coating showed epitaxial growth. This would also allow for a better control of diffusion processes, which is necessary for the thinner PVD coatings when compared to standard thermally sprayed bond coats. Subsequently to the substrate-like coating, an Al-Cr-O oxide layer is deposited, which may, in addition to acting as an oxidation barrier, replace the standard TGO layer. The whole layer stack is deposited in one PVD process. This means that there is no interruption of vacuum conditions in the transition between the substrate-like coating and the oxide. In previous investigations [16], we showed that quasi-epitaxial growth was achieved for the substrate-like coating on a polycrystalline substrate material. In this work, we deposit the PVD layer stack on a single-crystalline substrate and investigate the microstructure of the layer stack as obtained by in-situ processing and after annealing at 1100 °C.

2. Experimental

The deposition of the layer stack was performed in an industrial-size deposition system of the type INNOVA (Oerlikon Surface Solutions AG, Oerlikon Balzers), which is routinely used for coating tools and components. Non-reactive (without the addition of gases) as well as reactive (in pure oxygen atmosphere) cathodic arc evaporation (CAE) was utilized to create the layer stack in one in-situ process, i.e. without interruption of vacuum. The substrate is a PWA 1483 single crystal (SX) superalloy with a (001) crystallographic orientation (proprietary alloy of Pratt & Whitney). Samples with dimensions of (27 × 10 × 3) mm were cut from a larger piece of bulk material. Before deposition, the substrates were mechanically and chemically polished and wet-chemically cleaned. For deposition, the substrates were mounted on a two-fold rotating substrate holder.

Two types of targets were necessary to synthesize the layer stack. The first target type, referred to as superalloy target, was fabricated from powders (Oerlikon Surface Solutions AG, Oerlikon Metco) with a chemical composition listed in Table 1. This powder composition was selected to be identical with the composition of the PWA 1483 bulk material specified by Pratt & Whitney [17]. The composition of the powder was obtained by inductively coupled plasma optical emission spectrometry (ICP-OES) and inductively coupled plasma mass spectrometry (ICP-MS). It is assumed that this composition is also identical with the chemical composition of the superalloy substrate utilized in this investigation. The superalloy target was manufactured by spark plasma sintering (PLANSEE Composite Materials GmbH), a process which allows high sintering temperatures under high pressure. The composition was confirmed by energy dispersive X-ray spectroscopy (EDS), and it is shown in Table 1 that the chemical composition at the surface of the superalloy target after operation in the non-reactive mode is in good agreement with the chemical composition of the powders utilized for manufacturing.

Table 1
Chemical composition of the powder utilized for manufacturing the superalloy target and the chemical composition of the target surface after utilization in non-reactive arc evaporation.

Element	Ni	Co	Cr	Mo	W	Ta	Ti	Al	C
Powder Composition [wt%]	60.3	9.0	12.2	1.9	3.8	5.0	4.1	3.6	0.07
Target Composition [wt%]	59.9	9.1	14.3	1.3	3.6	5.5	3.1	3.2	n.a.

The second target type consists of Al and Cr with a composition of 70 at.% Al and 30 at.% Cr (referred to as $Al_{0.7}Cr_{0.3}$ target) manufactured from powders in a standard forging process at moderate temperatures (PLANSEE Composite Materials GmbH). Both targets have an identical size of Ø 150 mm. One of each target type was utilized in the deposition process. In the beginning, the process chamber was evacuated below 0.02 Pa and standard heating and etching steps were performed to ensure a sufficient coating adhesion to the substrate. The deposition started once the substrate temperature of 550 °C was reached. The superalloy target was operated with a DC arc current of 180 A, and a net deposition time of 12 min was chosen to form the substrate-like coating with a thickness of approximately 500 nm in the non-reactive process (metallic vapour only) on the PWA 1483-SX substrate. Subsequently, the transition to the oxide layer was performed in short sequence with the following steps: a) ignition of the $Al_{0.7}Cr_{0.3}$ target and evaporation with a DC arc current of 180 A while still operating the superalloy target - both in non-reactive mode, b) initiation of an oxygen flow of 400 sccm, c) switching-off the superalloy target. This sequence results in a transition coating thickness of about 100 nm. The targets were mounted opposite to each other in the coating chamber at the chamber walls. In the center of the chamber, a carousel was rotating with single rotation and at the carousel substrate holders with an additional rotation were mounted - resulting in a double rotation of the substrates. The transition layer with the multilayer structure shown in Fig. 1c is due to the double rotation of the substrate. When the substrate is during rotation in the vicinity of the superalloy target, it has higher Ni content, if it is in the vicinity of the $Al_{0.7}Cr_{0.3}$ target, the coating shows more Al. This part of the deposition process lasts only a few minutes. For the oxide coating, the $Al_{0.7}Cr_{0.3}$ target was operated at 180 A in an oxygen flow of 400 sccm. A symmetric bipolar bias voltage of 40 V with a frequency of 25 kHz and a negative pulse length of 36 μs and 4 μs positive pulse length was applied to the substrate during processing in oxygen. This resulted in a thickness of the Al-Cr-O of approximately 3.5 μm.

Transmission-EBSD (T-EBSD), also called Transmission Kikuchi Diffraction (TKD) analyses were performed in a dual FIB FEG-SEM Lyra3 from Tescan, using a Digiview IV EDAX camera, on lift-out specimens of ~100 nm thickness, mounted on a holder with a pre-tilt angle of 20° to the pole piece with 3 mm working distance. Beam conditions were 30 kV and 5 nA. The lift-out lamellae were also analyzed by transmission electron microscopy (TEM) in a JEOL JEM 2200 fs equipped with an EDAX system for EDS analysis.

Additional composition analysis was performed by Rutherford Backscattering Spectrometry (RBS) [18] at the EN tandem accelerator of the Federal Institute of Technology in Zurich. The measurements were performed using a 2 MeV, 4He beam and a silicon PIN diode detector under 168°. The collected data were evaluated using the RUMP program [19].

X-ray diffraction (XRD) measurements on the coating were performed on a Bruker D8 Discover Davinci diffractometer (Bruker AXS GmbH) equipped with a Göbel mirror for the generation of a parallel beam and with a LynxEye 1D detector using Cu-Kα radiation. The measurements were carried out in θ/2θ mode between 15° and 120° and in grazing incidence mode (ω = 1°) in the same 15° to 120° 2θ range.

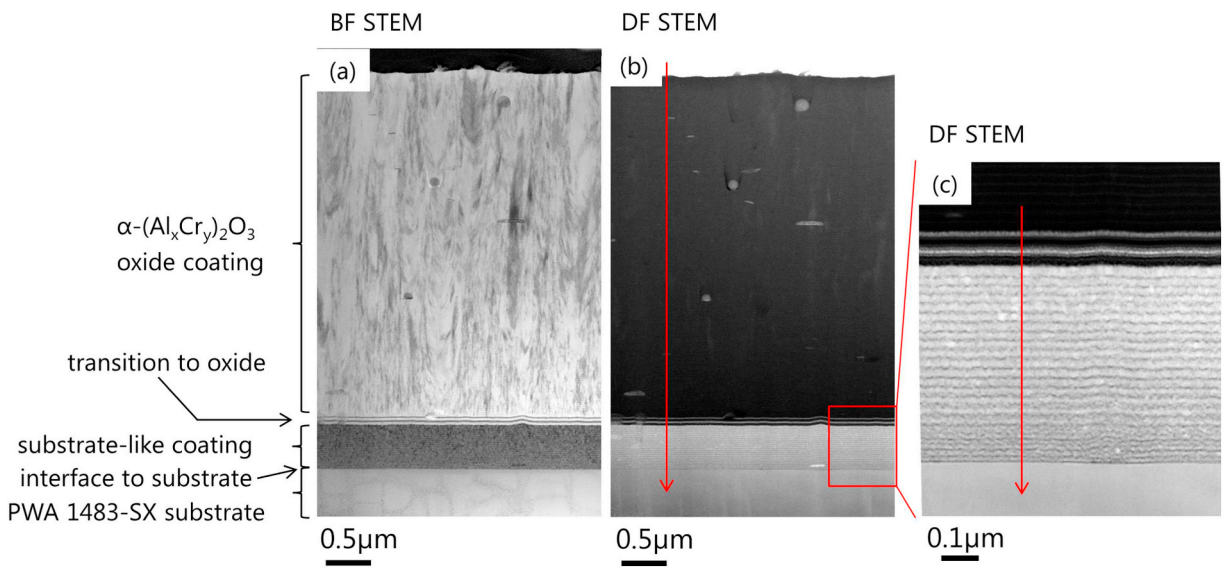

Fig. 1. a) BF STEM and b) DF STEM images of the cross section of a PWA 1483-SX substrate showing the γ/γ′ microstructure coated with the layer stack: substrate-like coating and $(Al_xCr_y)_2O_3$ oxide coating on top; the interface to the substrate is very distinct, whereas the transition to the oxide depends strongly on the deposition parameters, resulting in a transition region of ca. 100 nm. A magnified view of the substrate-like coating is shown in DF mode in c). Red arrows indicate positions of the EDS line scans shown in Fig. 2. (For interpretation of the references to colour in this figure legend, the reader is referred to the web version of this article.)

For phase analysis, the software Diffrac.Eva V4.1 from Bruker was used in combination with the crystal open database COD [20].

3. Results and discussion

Fig. 1 shows scanning transmission electron microscopy (STEM) images in a) bright-field (BF) and b) dark-field (DF) mode of a cross-section of the surface region of the substrate and the layer stack synthesized by CAE. The lower part of Fig. 1(a) shows the γ/γ′ microstructure of the substrate. The layered structure of the substrate-like coating, which can be seen in Fig. 1(c), is a result of the 2-fold substrate rotation during deposition. TEM indicates very small grains on the order of 10 nm and no indication of quasi-epitaxial growth for this region. Additionally, it can be recognized that, despite the constant conditions of the 2-fold rotation, the thickness of the bilayers in the substrate-like coating increases with time. This is due to a gettering effect of residual gases in the beginning of evaporation, which corresponds to a reduced evaporation rate. Subsequent to the substrate-like coating, the transition layer of ~100 nm is formed. It was realized by the additional ignition of the $Al_{0.7}Cr_{0.3}$ target and the addition of oxygen to the arc discharge after a few minutes. After stabilization of the oxygen flow, the superalloy target was switched off. The layered structure again indicates the influence of substrate rotation and the difference in brightness suggests different chemical composition in the two-layered structure. Nevertheless, the thickness of the substrate-like coating is very homogeneous. Finally, the operation of the $Al_{0.7}Cr_{0.3}$ target in the oxygen flow of 400 sccm results in the formation of an oxide coating. The cross section of this coating shows the presence of many columnar grains and numerous small droplets with spherical or flat geometry. These droplet shapes have been ascribed to Cr-rich and Al-rich regions [21,22], which act also as initiation sites for further grain growth.

The elemental composition of the cross section shown in Fig. 1 was investigated by EDS in the TEM. Fig. 2(a) shows the line scan for the entire layer stack. There is a clear trend of higher Cr content in the substrate-like coating compared to the bulk substrate. Additionally, there is oxygen in the coating and some indication for a slight increase in Co. As expected, the oxide coating (dark contrast) shows only the three elements Cr, Al and O, which come from the Al-Cr-O target. The enlarged EDS line scan of the substrate-like coating is displayed in Fig. 2(b). This line scan supports the hypothesis of oxygen diffusion into the substrate-like coating and it also suggests a much higher Cr content than what is expected from the condensation of the pure superalloy vapour. In addition, there is an indication that the Ni concentration increases slightly towards the oxide coating. The reason for this might be an instability in the transition region. Due to substrate rotation, regions with higher Ni and other substrate metal concentrations are formed in this thin transition region (bright contrast in DF STEM).

At the transition from oxide coating to substrate-like coating, one can also see a mild increase in Cr and a drop in Al concentration. However, there are neither Ni nor other traces of the PWA material detectable in the oxide coating. In other words, it seems likely that the transition to the oxide may cause non-controlled diffusion processes already during deposition. However, the RBS spectrum with a depth resolution of ca. 500 nm, which is shown in Fig. 3, does not show any

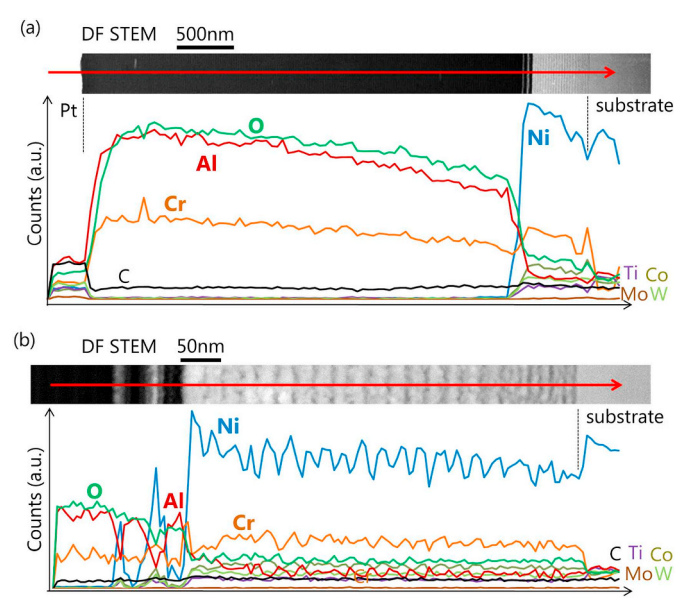

Fig. 2. DF STEM images and respective EDS line scans through a) the entire layer stack as indicated in Fig. 1(b) and b) the substrate-like coating with higher resolution as indicated in Fig. 1(c).

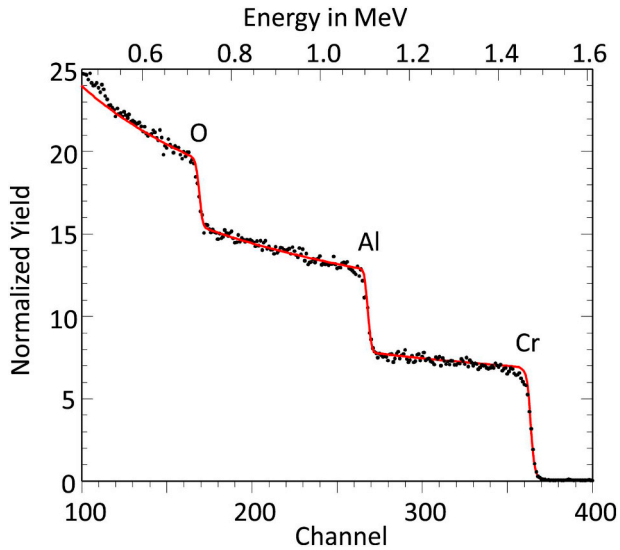

Fig. 3. RBS spectrum of the coating surface shown in Fig. 1 in the as-deposited state. The spectrum shows the oxide coating indicating a chemical composition of $(Al_{0.71}Cr_{0.29})_2O_3$.

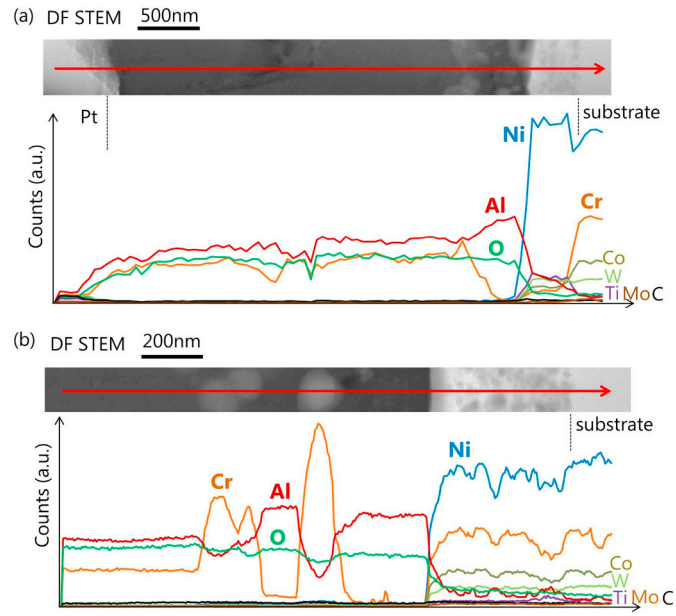

Fig. 5. DF STEM images and respective EDS line scans through a) the entire annealed layer stack as indicated in Fig. 4(b) and b) the substrate-like coating and lower region of the oxide coating with higher resolution as indicated in Fig. 4(c).

indication of elemental diffusion towards the surface of the oxide coating. Except for the Al, Cr and O signals, no other elements are visible. The analysis of the spectrum indicates an Al-Cr-O with $(Al_{0.71}Cr_{0.29})_2O_3$ composition, which is in excellent agreement with the metallic ratio of the $Al_{0.7}Cr_{0.3}$ target utilized for the oxide synthesis.

To test the thermal stability of the layer stack and of the interface to the substrate, a heat treatment was performed. The samples were annealed at 1100 °C with a heating rate of 10 °C/min, kept for 1 h at maximum temperature at ambient conditions and cooled down to room temperature with a cooling rate of 20 °C/min. Cross-sectional BF and DF analyses, Fig. 4(a) and (b) respectively, were performed to investigate the changes in the microstructure of the layer stack. The nano-layered structure, which was observed in the as-deposited state, recrystallizes in the entire substrate-like coating. In addition, the transition region to the oxide disappeared completely. The microstructure of the oxide coating changed as well and larger grains formed. The magnified DF STEM image in Fig. 4(c) illustrates the substrate-like coating and lower part of the oxide coating in more detail. The interface to the substrate is still very distinct and shows a clear change in microstructure from the substrate to the substrate-like coating. Despite of all oxidation and diffusion processes in the layer stack, the thickness of the substrate-like coating did not change and porosity was not observed.

EDS line scans were performed to analyze the change in chemical composition after the heat treatment. The arrow in Fig. 4(b) indicates the investigated region displayed in Fig. 5(a). Most striking is a rearrangement of the Al and Cr at both interfaces to the substrate and to the oxide. The analysis indicates a diffusion of Cr and Co into the substrate. Furthermore, there is a depletion of Cr visible at the interface to the oxide and an increase in the Al content. The enlarged EDS line scan in Fig. 5(b) (with reference to the indicated position in Fig. 4(c)) shows more details about the rearrangement in the interface regions after annealing. Adjacent to the substrate-like coating, a pure alumina

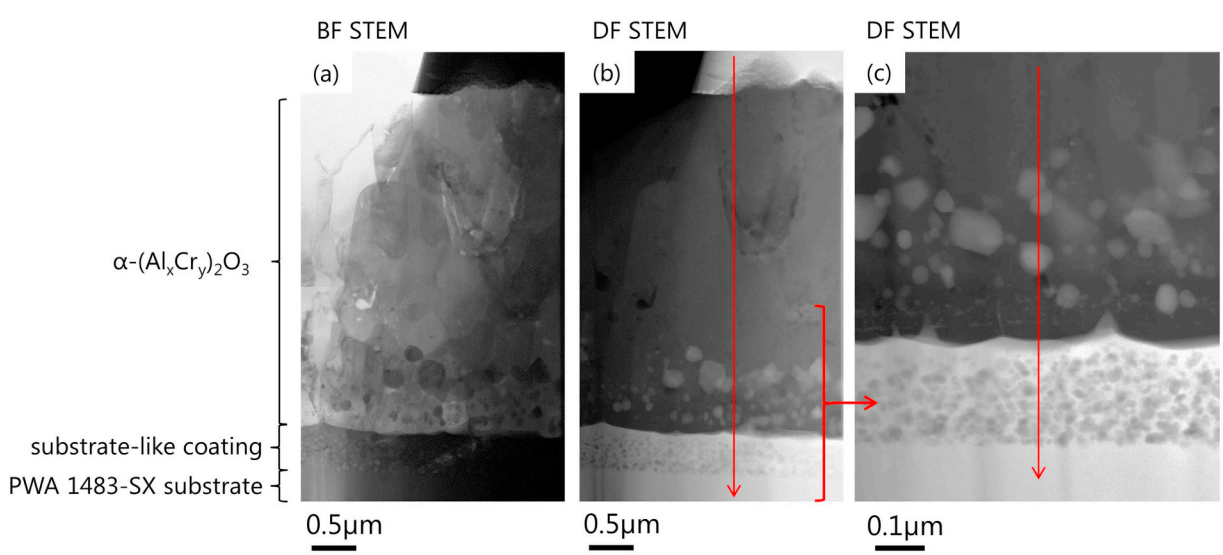

Fig. 4. a) BF STEM, b) DF STEM images of the layer stack after annealing of 1 h at 1100 °C in air and c) DF STEM image with higher magnification. The red arrows indicate locations of the EDS line scans shown in Fig. 5. (For interpretation of the references to colour in this figure legend, the reader is referred to the web version of this article.)

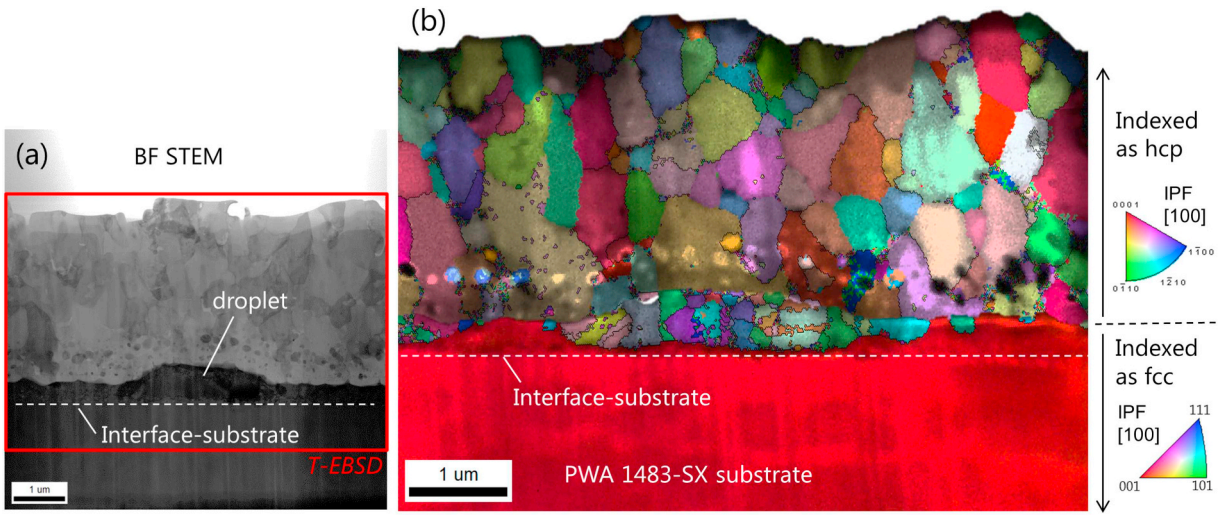

Fig. 6. a) BF STEM image of a cross section of the annealed layer stack. The red rectangle indicates the location of the b) T-EBSD analysis showing an overlay of the T-EBSD pattern quality and crystal orientation maps. The substrate-like coating shows epitaxial recrystallization on the superalloy substrate, except at the droplet, which was also indexed as fcc. The oxide coating, which was indexed as hcp, recrystallized into a more globular grain morphology. (For interpretation of the references to colour in this figure legend, the reader is referred to the web version of this article.)

region is formed. By means of T-EBSD, shown in Fig. 6, the structure of this alumina was identified to be corundum. Further, the line scan indicates a region in which the corundum coexists with Cr-enriched oxide phases. Above this region and towards the surface of the layer stack, a $(Al,Cr)_2O_3$ solid solution with corundum structure was formed, i.e. with the same crystal structure as the α-alumina.

T-EBSD measurements as shown in Fig. 6 allow for a detailed characterization of the layer stack after annealing. In contrast to our previous depositions on spark plasma sintered bulk material obtained from powder with PWA 1483 composition [16], no in-situ epitaxial growth was achieved here prior to heat treatment. This indicates that the polycrystalline surface is more favorable - probably due to a multitude of crystalline orientations - to offer the energetically most favored orientation for nucleation and growth according to the crystal structure of the substrate.

The T-EBSD analysis performed after the heat treatment confirms that the substrate-like coating and also the droplet at the interface to the substrate share the same lattice structure (cubic *fcc*) as expected from the superalloy substrate. The position of the interface to the substrate is indicated by the dashed line. Additionally, the T-EBSD analysis confirms that a large part of the substrate-like coating recrystallizes with the same orientation as the PWA 1483 substrate.

At the interface to the oxide, pure α-Al_2O_3 with some Cr-enriched phases of globular morphology but of unknown crystallographic structure (bright contrast in the DF STEM images) are formed in a region of ca. 600 nm in thickness. Besides the formation of the α-Al_2O_3 towards the superalloy material, another interesting result of the thermal treatment is that the T-EBSD map shows for the α-Al_2O_3 at the interface to the oxide exactly the same grain structure (hcp) and orientation as for the α-$(Al_xCr_y)_2O_3$ phase on top of the layer stack. The α-$(Al,Cr)_2O_3$ phase recrystallized into grains with a size of ca. 700 nm.

The RBS analysis of the surface of the layer stack after annealing, which is presented in Fig. 7, shows also some important differences compared to the as-deposited state. In addition to the expected Al, Cr and O from the Al-Cr-O, a Ni peak (not distinguishable from Co) < 1.2 at.% is visible in the spectrum, indicating that small amounts of Ni diffuse to the surface of the layer stack during annealing. This concentration is below the EDS detection limit. It is assumed that this Ni originates from the transition region, which was originally formed in the as-deposited state (Fig. 2(b)). There the Ni concentration was locally increased due to substrate rotation and different positions of the superalloy target and $Al_{0.7}Cr_{0.3}$ target in the deposition system.

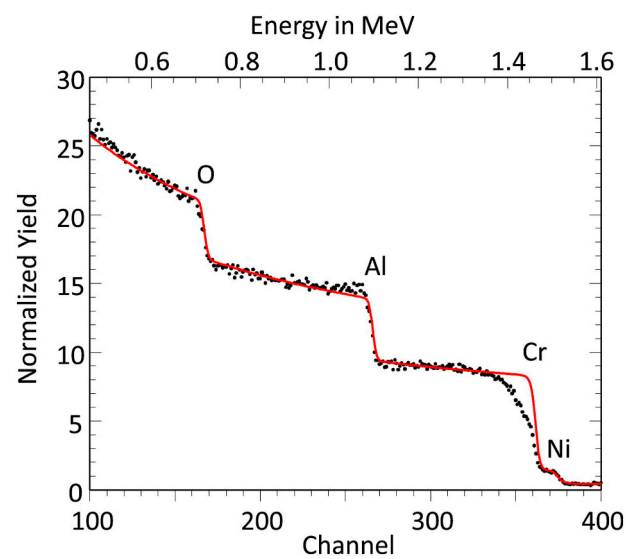

Fig. 7. RBS spectrum of the annealed layer stack surface showing O, a mild increase in Al, depletion of Cr and very low amounts of Ni in the oxide coating.

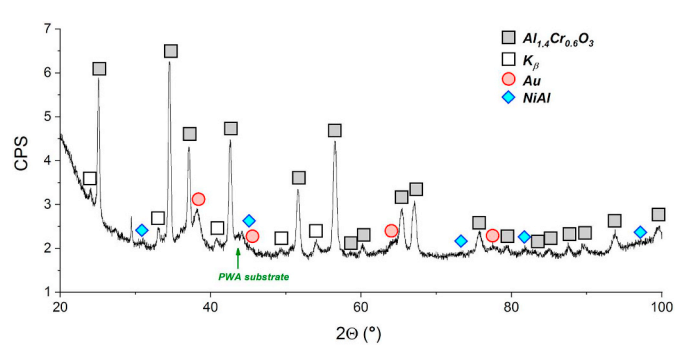

Fig. 8. Grazing-incidence XRD measurement of the annealed layer stack.

However, the reservoir of elements for such diffusion processes is very limited. Besides, the RBS analysis shows depletion of Cr at the surface of the oxide coating and a slight increase in Al.

Fig. 8 shows a grazing incidence XRD measurement of the annealed

layer stack. In this case, no Ni filter was used, in order to increase the overall intensity. The dominant peaks belong to the corundum structure of the $(Al,Cr)_2O_3$ solid solution. Some K_β peaks are also visible. The presence of gold is explained by the previous FIB/SEM analysis, for which the specimen had to be coated by a thin Au film of a few nm for conductivity reasons. Especially interesting are the small peaks belonging to the NiAl phase. These show that Ni diffuses in low amounts to the surface region of the oxide coating and forms the intermetallic compound of the B2 phase NiAl. The results are in agreement with the RBS data which show the presence of Ni, a local increase of Al and a decrease of Cr.

4. Conclusion

A layer stack of two components was deposited on a PWA 1483-SX substrate by cathodic arc evaporation, in a single process, i.e. without interruption of vacuum. For this, two targets were operated subsequently. The first layer was deposited using a target with the same nominal composition as the superalloy substrate. Then the deposition was switched over to a second target containing Al and Cr with a composition of 70 at.% Al and 30 at.% Cr in reactive mode under a constant flow of oxygen gas. This type of deposition resulted in an amorphous substrate-like coating with a thickness of ca. 500 nm and an α-$(Al_xCr_y)_2O_3$ oxide coating with columnar grain structure on top. As was confirmed by EDS line scans, the respective layers showed quite homogeneous chemical distributions according to the deposition parameters and only at the transition from the substrate-like coating to the oxide coating some diffusion processes occurred due to 2-fold substrate rotation and simultaneous operation of the two targets for a short duration.

After annealing of the layer stack at 1100 °C for 1 h at ambient conditions, it was confirmed that α-alumina was formed, which has the same grain structure (hcp) and orientation as the α-$(Al_xCr_y)_2O_3$ solid solution. The substrate-like coating, which recrystallized at elevated temperature, showed epitaxial growth on the superalloy single crystal according to T-EBSD measurements. This is already a good indication for a mechanically stable and well-adhered coating. Furthermore, the thickness of each layer of the layer stack remained the same and porosity was not observed. As was confirmed by RBS and XRD measurements, only small amounts of Ni diffused towards the top of the coating to locally form there the intermetallic compound of the B2 phase NiAl. This Ni originated from the transition region and it is believed that the Ni diffusion stops once the concentration gradient at the interface to the oxide becomes zero. This could mean that the diffusion process and the thickness of the corundum formed in the interface to the substrate-like coating can be controlled by the transition layer to the oxide. Due to the formation of corundum, it is furthermore expected that the annealed layer stack can be utilized as a diffusion and oxidation barrier. Based on the fact that corundum has the same hexagonal crystal structure as Al-Cr-O it can be expected that thick and stable barrier coatings can be realized with this material system. These results demonstrate the potential of CAE for the synthesis of oxides with barrier properties at high temperatures.

Acknowledgements

Kim von Allmen is gratefully acknowledged for additional XRD measurements. The financial support from Swiss CTI contract No. 17973.2 PFEN-NM is gratefully acknowledged.

References

[1] C.T. Sims, N.S. Stoloff, W.C. Hagel, I.I. Superalloys, High-Temperature Materials for Aerospace and Industrial Power, John Wiley & Sons, 1987.
[2] T.M. Pollock, S. Tin, Nickel-based superalloys for advanced turbine engines: chemistry, microstructure and properties, J. Propuls. Power 22 (2006) 361–374, https://doi.org/10.2514/1.18239.
[3] R.C. Reed, The Superalloys: Fundamentals and Applications, Cambridge University Press, 2006.
[4] M. Durand-Charre, The Microstructure of Superalloys, CRC Press, 1998.
[5] S. Neumeier, J. Ang, R.A. Hobbs, C.M.F. Rae, H.J. Stone, Lattice misfit of high refractory ruthenium containing nickel-base superalloys, Adv. Mater. Res. (2011), https://doi.org/10.4028/www.scientific.net/AMR.278.60.
[6] P. Caron, T. Khan, Evolution of Ni-based superalloys for single crystal gas turbine blade applications, Aerosp. Sci. Technol. 3 (1999) 513–523, https://doi.org/10.1016/S1270-9638(99)00108-X.
[7] M.J. Pomeroy, Coatings for gas turbine materials and long term stability issues, Mater. Des. 26 (2005) 223–231, https://doi.org/10.1016/j.matdes.2004.02.005.
[8] Y. Koizumi, T. Kobayashi, T. Yokokawa, J. Zhang, M. Osawa, H. Harada, Y. Aoki, M. Arai, Development of next-generation Ni-Base single crystal Superalloys, Superalloys 2004, TMS, 2004, pp. 35–43, , https://doi.org/10.7449/2004/Superalloys_2004_35_43.
[9] H.T. Pang, R.A. Hobbs, H.J. Stone, C.M.F. Rae, A study of the effects of alloying additions on TCP phase formation in 4th generation nickel-base single-crystal superalloys, Adv. Mater. Res. 278 (2011) 54–59, https://doi.org/10.4028/www.scientific.net/AMR.278.54.
[10] M. Peters, C. Leyens, U. Schulz, W.A. Kaysser, EB-PVD thermal barrier coatings for aeroengines and gas turbines, Adv. Eng. Mater. 3 (2001) 193–204, https://doi.org/10.1002/1527-2648(200104)3:4<193::AID-ADEM193>3.0.CO;2-U.
[11] D.V. Rigney, R. Viguie, D.J. Wortman, D.W. Skelly, PVD thermal barrier coating applications and process development for aircraft engines, J. Therm. Spray Technol. 6 (1997) 167–175, https://doi.org/10.1007/s11666-997-0008-6.
[12] G.W. Goward, D.H. Boone, Mechanisms of formation of diffusion aluminide coatings on nickel-base superalloys, Oxid. Met. 3 (1971) 475–495, https://doi.org/10.1007/BF00604047.
[13] Y. Tamarin, Protective Coatings for Turbine blades, ASM International, Materials Park, Ohio, 2002.
[14] N.P. Padture, M. Gell, E.H. Jordan, Thermal barrier coatings for gas-turbine engine applications, Science 296 (2002) 280–284, https://doi.org/10.1126/science.1068609.
[15] D.R. Clarke, S.R. Phillpot, Thermal barrier coating materials, Mater. Today 8 (2005) 22–29, https://doi.org/10.1016/S1369-7021(05)70934-2.
[16] J. Ast, M. Döbeli, A. Dommann, M. Gindrat, X. Maeder, A. Neels, P. Polcik, M.N. Polyakov, H. Rudigier, K.D. von Allmen, B. Widrig, J. Ramm, Synthesis and characterization of superalloy coatings by cathodic arc evaporation, Surf. Coat. Technol. 327 (2017) 139–145, https://doi.org/10.1016/j.surfcoat.2017.07.061.
[17] D.M. Shah, A. Cetel, Evaluation of PWA1483 for large single crystal IGT blade applications, Superalloys 2000 (Ninth International Symposium), TMS, 2000, pp. 295–304, , https://doi.org/10.7449/2000/Superalloys_2000_295_304.
[18] W.K. Chu, J.W. Mayer, M.A. Nicolet, Backscattering Spectrometry, Academic Press, 1978.
[19] L.R. Doolittle, A semiautomatic algorithm for Rutherford backscattering analysis, Nucl. Instrum. Methods Phys. Res., Sect. B 15 (1986) 227–231, https://doi.org/10.1016/0168-583X(86)90291-0.
[20] S. Gražulis, A. Daškevič, A. Merkys, D. Chateigner, L. Lutterotti, M. Quirós, N.R. Serebryanaya, P. Moeck, R.T. Downs, A. Le Bail, Crystallography Open Database (COD): an open-access collection of crystal structures and platform for world-wide collaboration, Nucleic Acids Res. 40 (2012) D420–D427, https://doi.org/10.1093/nar/gkr900.
[21] C.M. Koller, J. Ramm, S. Kolozsvári, J. Paulitsch, P.H. Mayrhofer, Role of droplets and iron on the phase formation of arc evaporated Al–Cr-oxide coatings, Surf. Coat. Technol. 276 (2015) 735–742, https://doi.org/10.1016/j.surfcoat.2015.05.012.
[22] C.M. Koller, R. Hahn, B. Widrig, J. Ramm, S. Kolozsvári, J. Paulitsch, P.H. Mayrhofer, Triggering the phase evolution within $(Al,Cr)_2O_3$-based coatings by alloying and microstructural concepts, Berg-Huettenmaenn. Monatsh. 161 (2016) 325–329, https://doi.org/10.1007/s00501-016-0506-2.